Evidence from Meteosat imagery of the interaction of sting jets with the boundary layer

Meteorol. Appl. 11, 277–289 (2004) DOI:10.1017/S1350482704001379

Evidence from Meteosat imagery of the interaction of sting jets with the boundary layer

K. A. Browning & M. Field
Joint Centre for Mesoscale Meteorology, Department of Meteorology, University of Reading, PO Box 243, Reading, Berkshire, RG6 6BB, UK
Email: k.a.browning@reading.ac.uk

Meteosat infra-red imagery for the Great Storm of October 1987 is analysed to show a series of very shallow arc-shaped and smaller chevron-shaped cloud features that were associated with damaging surface winds in the dry-slot region of this extra-tropical cyclone. Hypotheses are presented that attribute these low-level cloud features to boundary-layer convergence lines ahead of wind maxima associated with the downward transport of high momentum from overrunning, so-called sting-jet, flows originating in the storm's main cloud head.

1. Introduction

Building on forecasting experience reported by Grønås (1995), Browning (2004) has reanalysed the Great October 1987 Storm in south-east England to show that the most damaging winds occur in a distinct location within the dry slot at the tail-end of a bent-back front and cloud head – the 'sting at the end of the tail'. A cloud head and dry slot are well-known features of the satellite imagery from rapidly deepening extra-tropical cyclones (Böttger et al. 1975; Browning & Roberts 1994); they are characteristic of cyclones that follow the evolution described in the model of Shapiro & Keyser (1990). A distinct mesoscale phenomenon referred to as the sting jet is thought to be responsible for the damaging winds in the dry slot: Clark & Browning (2004) have carried out a high-resolution numerical-weather-prediction modelling study of the Great October Storm to show that the sting jet originates within the cloud head at mid-tropospheric levels and that it accelerates rapidly over a 3-hour period, reaching about $50\,m\,s^{-1}$ as it descends towards the boundary layer.

Figure 1 shows a pair of model-derived soundings obtained in the study by Clark & Browning (2004) along the descending trajectory of a parcel within the sting jet. Table 1 gives a summary of the changes in the properties of the sting-jet observed between the two soundings which were obtained three hours apart. The flow in the sting jet is seen to increase from $20\,m\,s^{-1}$ to $50\,m\,s^{-1}$ over the three hours as it descends from 5 km to 2 km. The air warms to some extent by dry adiabatic descent and so reaches the 2-km level above a strong temperature inversion. This by itself would tend to increase the Richardson number and thereby reduce the shearing instability and associated transport of high momentum to the surface. However, Table 1 shows that the air is 5 K colder than it otherwise would have been by entirely dry adiabatic descent because of an evaporative heat sink, thereby reducing the Richardson number. This is consistent with the suggestion by Browning (2004) that evaporation may play a role in increasing the strength of the damaging wind gusts at the surface. The magnitude of the surface gusts is sensitive both to the processes that generate the sting jet and also to the processes that transport the high momentum of the sting jet downwards through the inversion-capped boundary layer. The purpose of the present paper is to describe some satellite observations of mesoscale structures that are thought to be associated with these transport processes.

Clark & Browning (2004), in their study of the Great October Storm, employed a model with a 12-km grid which was able to resolve the sting jet and to show that it was part of a slantwise convective circulation within the curved tip of the cloud head; however, the model did not fully resolve the mesoscale substructure of this circulation. According to the observational study by Browning (2004), the cloud-head circulation is believed to be in the form of multiply stacked slantwise circulations as shown by the conceptual model in Figure 2. The multiple descending branches (stippled arrows) in this model correspond to multiple sting jets, or multiple wind maxima within the overall sting jet, and it is these flows that enter the dry-slot region where they interact with the boundary layer and give rise to damaging surface winds. The present paper examines Meteosat infra-red imagery which not only reveals the sub-structure associated with the multiple cloud-head flows but also reveals characteristic patterns of low-level cloud in the dry slot that are associated with vertical-transport processes within the boundary layer

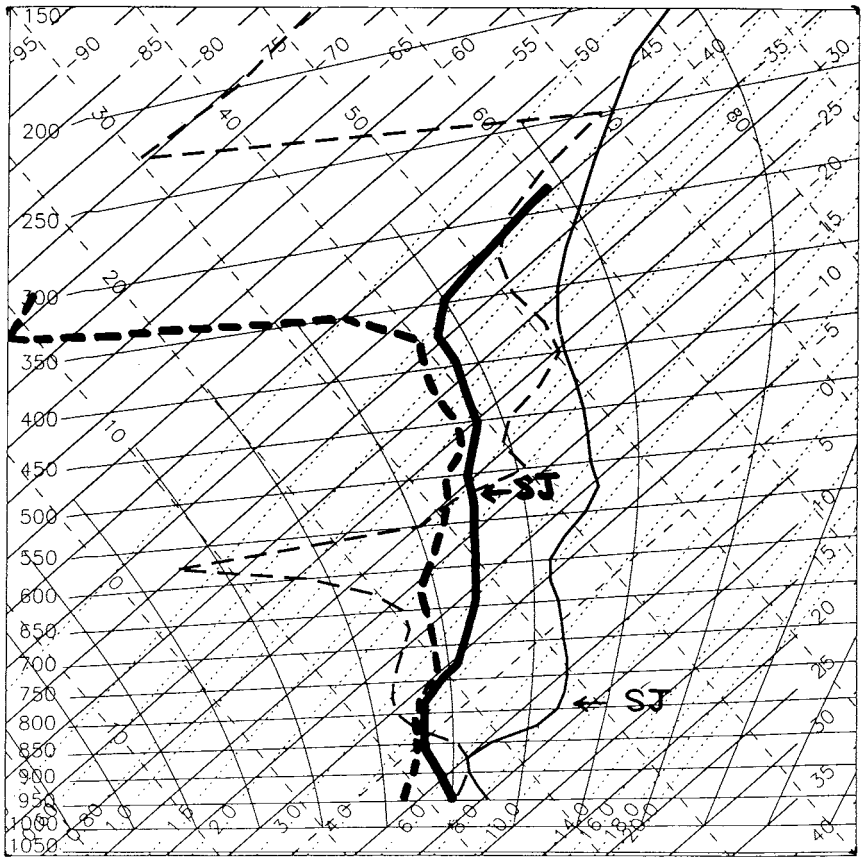

Figure 1. *Pair of model-derived soundings derived in the study by Clark & Browning (2004) for locations along the trajectory of a parcel within the descending sting-jet flow. Soundings plotted as thick lines correspond to the time when the air parcel in the sting jet (SJ) was just above 550 mb (5 km). The thin lines correspond to the time 3 hours later when the same parcel had descended to 800 mb (2 km). Solid and dashed lines represent dry-bulb and dew point temperatures, respectively.*

Table 1. *Properties of a parcel within the sting jet at the beginning and end of the 3-hour interval between the two soundings in Figure 1.*

	Initial value	End value
Height (km)	5	2
Pressure (mb)	550	800
Velocity ($m\,s^{-1}$/deg)	20/230	50/240
Dry-bulb potential temperature (K)	T	T-5
Wet-bulb potential temperature (K)	285	285
Mixing ratio ($g\,kg^{-1}$)	M	M + 1.8

and appear to be related to the multiple cloud-head flows.

2. Analysis of satellite imagery on 16 October 1987

The area of most damaging winds on 16 October reached the Channel Islands and central southern England at around 0130 UTC and then propagated eastwards and northwards, reaching Sussex and the London area by 0300 UTC, and Kent and the coast of East Anglia by 0430 UTC. The analysis is therefore focused on the period 0130 to 0430 UTC, during which half-hourly infra-red images were available from Meteosat. In order to extract the required information, two image enhancement schemes, referred to as E1 and E2, have been adopted. In scheme E1 a range of brightness temperature between 275 K and 235 K is employed to reveal the substructure of the major mid- and upper tropospheric cloud features associated with the cloud head. However, to reveal the structure of the low-level clouds believed to be associated with boundary layer convergence lines within the dry slot, the image grey-scale in the E2 scheme is concentrated within the narrow range of brightness temperature from 265 K to 280 K.

2.1. Overview of the satellite analyses

Figures 3a and 3b show E1-enhanced images for 0130 and 0230 UTC, respectively. Information inferred from these images and from other sources is overlaid. The red lines represent the axes of the main cloud-head bands, a, b and c (although, as pointed out later, each of these bands had a rapidly evolving fine structure). Band a had developed much earlier and was decaying at the outer edge of the cloud head at this time. Bands b and c are the dominant cloud bands, with c being

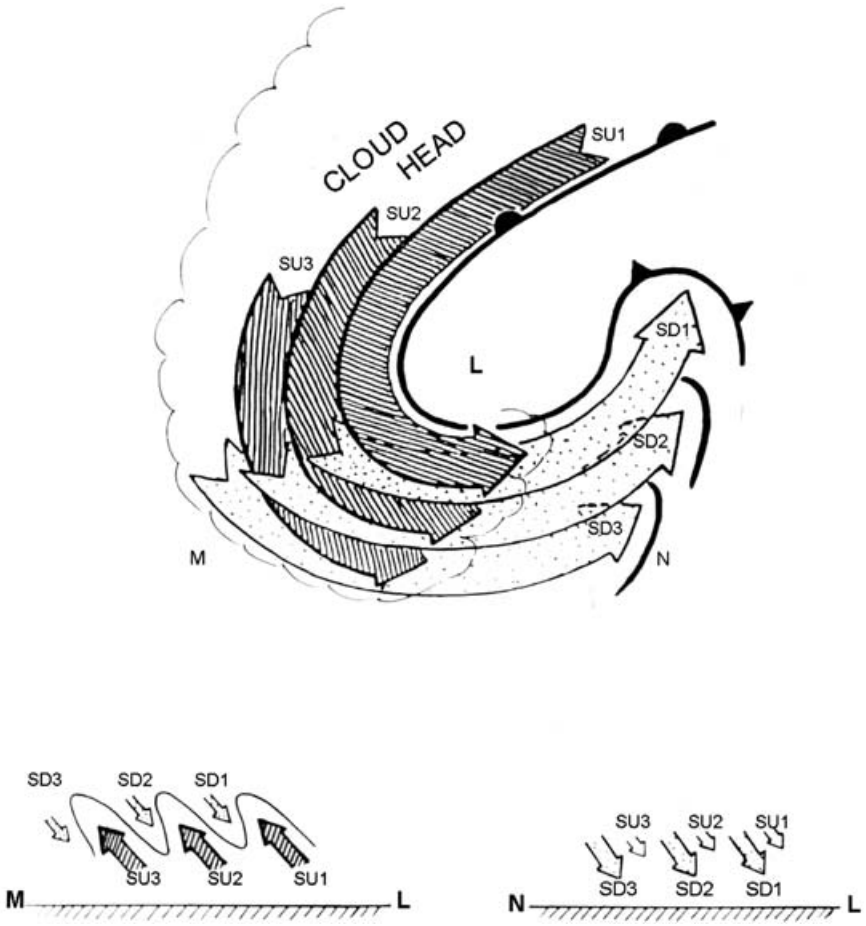

Figure 2. *Conceptual model depicting stacked slantwise convective circulations wrapping around the bent-back front of an intense extratropical cyclone. The cyclone is shown at the stage of minimum central pressure when the bent-back front (thick line) has almost encircled warm air near the cyclone centre (L). The main diagram shows a plan view in which three slantwise convective circulations are sketched, each consisting of a slantwise ascending, SU (hatched), and a slantwise descending, SD (stippled), branch. As shown in the vertical cross-sections along ML and NL, in the bottom left and right corners, respectively, each (SU + SD)-pair can be interpreted as a transverse circulation (radially outward from the cyclone centre) which is superimposed on the strong flow along the axis of the plan-view arrows approximately parallel to the bent-back front. The SU parts of these circulations are cloudy with precipitation in the region represented by the cross-section ML, and they are collectively responsible for the hooked tip of the cloud head. Descent dominates in both branches of the circulations beyond the tip of the cloud head, i.e. in the region represented by the cross-section NL. The evaporatively cooled air, especially that within the SD parts of the circulations, descends towards the boundary layer, leading to the very strong surface wind gusts that occur near and just ahead of the tip, or tail-end, of the cloud head. These winds are referred to as 'the sting at the end of the tail.' (From Browning 2004.)*

the most recently formed of the three labelled bands. Many other bands (some are shown in red but not labelled) exist to the north of c, the newest ones being generated along the warm front (see bands over northern England). Following the arguments given in Browning (2004), it is hypothesised that each of these bands was associated with a transverse circulation consisting of a layer of slantwise ascent above a slantwise descending flow. The propagation of the cloud bands suggests that successive transverse circulations form close to the bent-back and warm fronts and propagate outwards towards the outer edge of the cloud head. As the banded circulations move towards the tip of the cloud head, into the positions of bands c and b, the descending limbs of the circulations accelerate to give the strong slantwise descending sting-jet flows modelled by Clark & Browning (2004). Although several sting jets may coexist as part of this array of circulations, it is suspected that at any given time one or perhaps two of the sting jets will dominate.

Also shown in Figures 3a and 3b are surface frontal analyses (green lines) which depict the late stages in the seclusion of a pocket of warm moist air close to the cyclone centre as cold air begins to circulate around it, as in the model of Shapiro & Keyser (1990: fig. 10.27). The frontal analyses are based on analyses of surface observations as described in the Appendix. The warm seclusion and cyclone centre are situated just within the dry slot, and the cloud-head bands, a, b and c, can be seen terminating at the tip of the cloud head just to the south of it. The strongest surface wind gusts were ahead of the tips of cloud-head bands b and c in a region centred on the small white asterisk in Figure 3a. For a detailed surface wind analysis at this time, see Browning (2004: fig. 9).

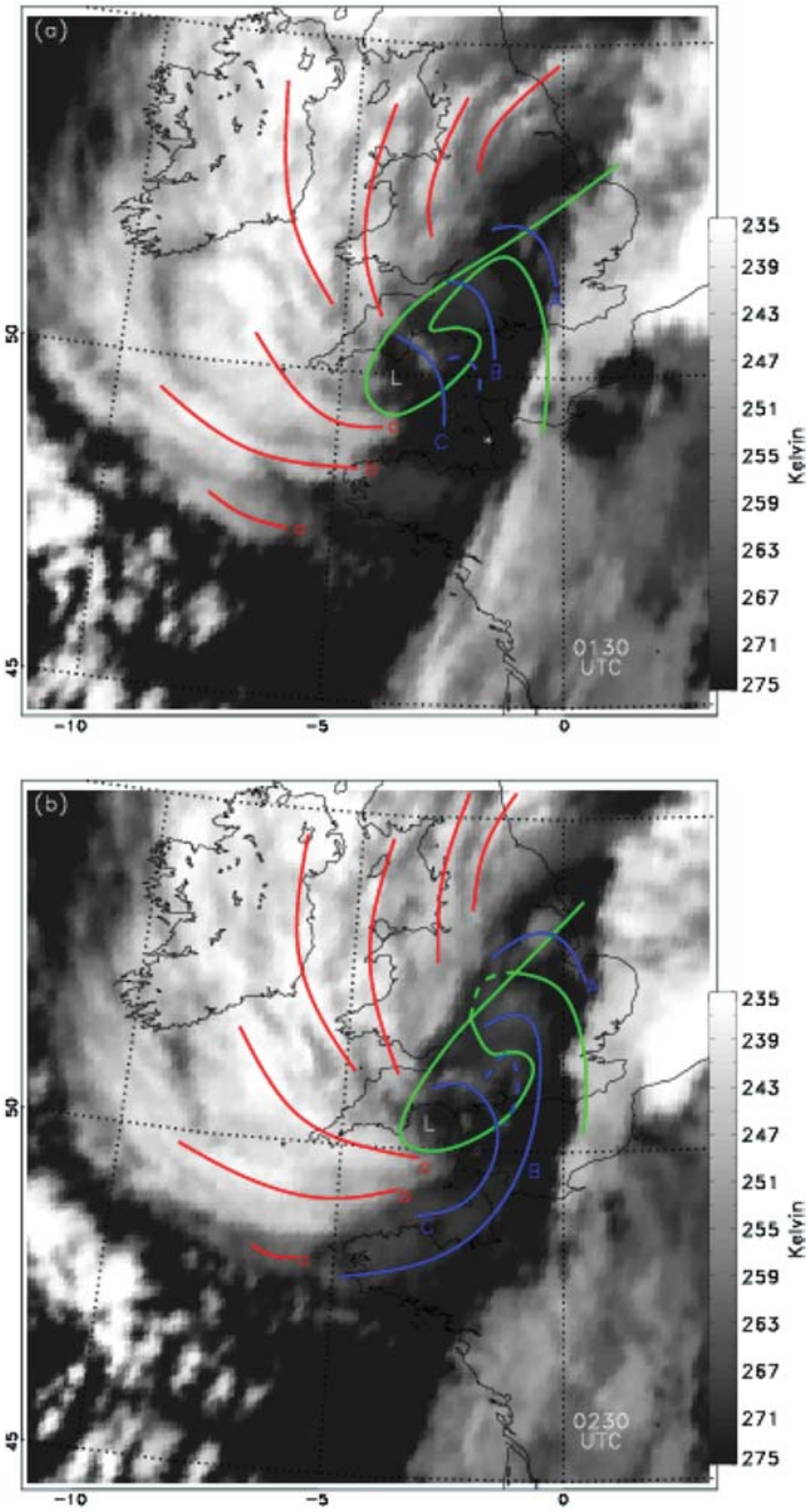

Figure 3. *Meteosat infra-red images for (a) 0130 UTC and (b) 0230 UTC, 16 October 1987, using the E1 enhancement scheme to show the structure of the middle- and high-level cloud. Axes of three cloud-head bands, a, b and c (and four others), are denoted by red lines. The blue lines, labelled A, B and C, show the axes of boundary-layer convergence lines inferred from Figure 4. The green lines show the surface frontal analysis as explained in the text. L is the surface low-pressure centre and the small white asterisk in (a) denotes the centre of the region of strongest surface winds.*

The blue thin lines in Figures 3a and 3b show the positions of dry-slot cloud features seen in the E2-enhanced imagery. We shall show that their behaviour is consistent with the hypothesis that they are due to boundary-layer convergence lines. These lines are labelled A, B and C, in the belief that they are related to the multiple sting jets associated with cloud bands a, b and c, respectively. This is consistent with the hypothesis in Browning (2004) – and encapsulated in Figure 2 in the present paper – that, following the evaporation of the associated cloud and precipitation, the leading edges of the multiple sting jets advance through the dry-slot region. Although it is not possible to be sure of a one-to-one relationship between A and a, B and b, C and c, etc., it is plausible to associate the oldest decaying band, a, with a convergence line at the leading edge of the first outflow, A, which has travelled furthest away from the tip of the cloud head, and to associate the newest band, c, with the latest outflow, C, which has progressed only a short distance away from the tip of the parent cloud head.

2.2. The arc-shaped cloud lines within the dry slot

The evidence used to draw the blue curves representing shallow cloud lines A, B and C in Figure 3 was obtained from E2-enhanced infra-red images. Two of these images are reproduced in Figure 4. The black lines, which correspond to the blue lines in Figure 3, are drawn through the brightest (coldest) parts of the arc-shaped cloud features believed to be due to convergence lines. Lines B and C are characterised by diffuse arcs of stratiform cloud, presumably capped by the inversion at the top of the boundary layer (although there is a hint of some very shallow convective cells along line C). Radar network pictures (not shown) indicate that there was some rain along parts of lines B and C but it was mainly light. Line A was different in that it consisted of slightly deeper convective cells which produced heavy rain showers as discussed in Browning (2004). Line A, related to the cold front, is shown as ahead of the cold front in Figure 3 because it is drawn through the middle of the clusters of cumulonimbus clouds (see Figure 4): the upwind ends of these clouds were in fact close to the cold front.

The precise shape of parts of the curves drawn in Figures 4a and 4b might seem a little arbitrary from inspection of the individual figures but can be justified from continuity considerations when looking at the full sequence of images. The successive positions of lines A, B and C are drawn in Figures 5a, 5b and 5c, respectively. Figure 5d shows the time of maximum observed surface gusts from which it is clear that most of the strongest gusts occurred close to the passage of line B. Others occurred about two hours behind line C. Only one station, in central southern England, experienced its strongest gusts in association with line A.

The nature of the clouds associated with each of the arc-shaped cloud bands is, as noted above, different for the different lines, but the sting-jet flows are thought to be a common ingredient of all of them. The cumulonimbus clouds forming along line A were due to the triggering of potential instability where sting-jet air overran air with higher wet-bulb potential temperature (θ_w) (within the W2 flow as discussed by Browning (2004)). The stratiform arc clouds B and C were due to lines of boundary-layer convergence, which it is hypothesised were being generated at the leading edges of regions of enhanced downward transport of high momentum (through turbulence and gravity waves rather than convection) beneath the overrunning sting-jet flows.

There are two opposing factors to consider in the generation of cloud along lines B and C. On the one hand, the downward transport of momentum from each overrunning sting-jet will tend to have generated an arc of convergence at its leading edge and hence also cloud because of the relatively high humidity within the boundary layer. On the other hand, to the extent that there was downward transport of mass as well as of momentum, this will tend to have dissipated the cloud because of the dryness of the descending sting-jet air. Figures 3a and 3b showed that the northern parts of the low-level convergence lines (B and C) were within the surface-based warm seclusion whilst their southern parts were within the low-θ_w flow that was encircling the warm seclusion. Surface observations showed that the air in the warm seclusion was close to saturation whereas the low-θ_w flow tended to be in the range of 60 to 80%, indicating that this was a region where dry air was indeed being mixed down. It was here, i.e. outside the south-east boundary of the warm seclusion and close to where the boundary-layer cloud arcs tended to dissipate, that the strongest surface gusts were recorded.

2.3. Small chevron-shaped cloud features within the dry slot

The arc-shaped cloud lines described in section 2.2 were over 100 km in length. Other notable stratiform cloud features observed in the dry slot were only a few tens of kilometres across. These small features were chevron-shaped, with a narrow belt of boundary-layer cloud, followed sometimes by a cloud-free pocket. Occasionally the chevron shape was more evident in the pattern of the cloud-free pocket than in the pattern of cloud itself. Chevron-shaped features were first observed clearly around 0230 UTC (see dashed feature near the Isle of Wight in Figure 4b) and they became more numerous after 0300 UTC, when the most damaging winds occurred in south-east England. Examples are given in Figures 6 and 7.

Figures 6a and 6b, respectively, show E2- and E1-enhanced versions of the imagery for 0300 UTC. Three

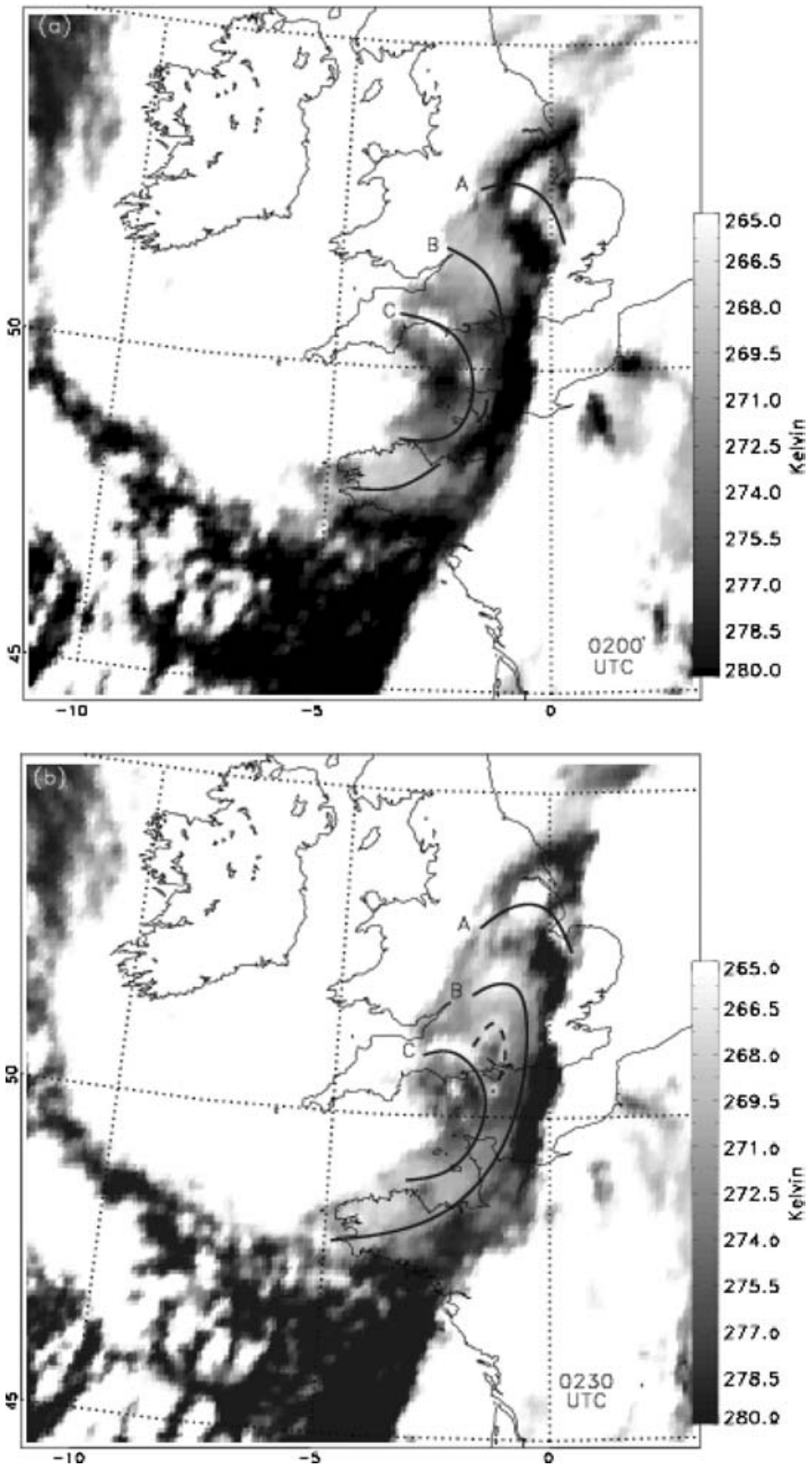

Figure 4. *Meteosat infra-red images for (a) 0200 UTC and (b) 0230 UTC, 16 October 1987, using the E2 enhancement scheme to reveal the structure of boundary-layer clouds. The superimposed black lines represent the estimated positions of boundary-layer convergence lines A, B and C inferred from the associated cloud patterns.*

chevron-shaped cloud features can be seen in Figure 6a, their locations being indicated by the blue dashed curves in Figure 6b (along with the positions of the arc-shaped cloud lines A, B and C and the cloud-head bands a', b and c, all of which are denoted by solid curves). The best-defined chevron is the one approaching Shoreham on the south coast of England (marked by x in Figure 6a). During the ensuing hour, there were several gusts exceeding $45\,\mathrm{m\,s^{-1}}$ (90 knots) at Shoreham, culminating with the anemometer being broken by

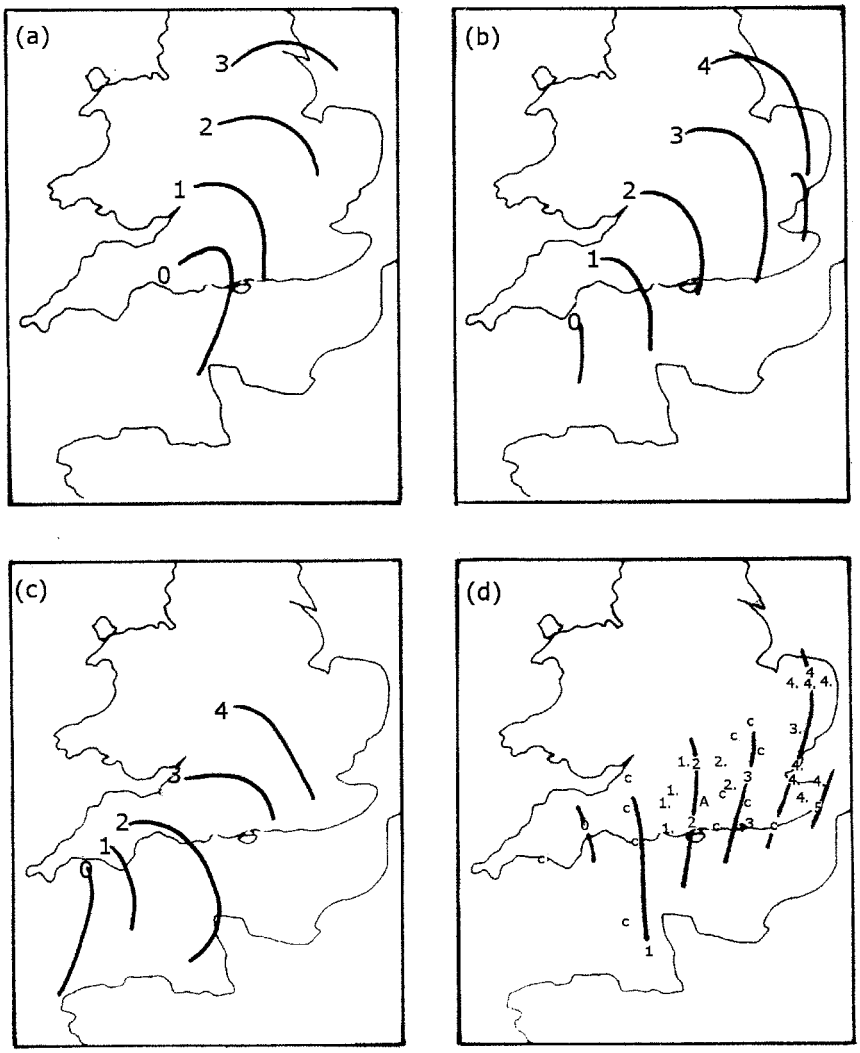

Figure 5. *Successive hourly positions of cloud features obtained from a sequence of images similar to those in Figure 4: (a) the line of convective cells labelled A; (b) the arc-shaped cloud line, B; and (c) the arc-shaped cloud line, C; all of which are interpreted as representing boundary-layer convergence lines. Panel (d) shows times of peak gusts recorded at stations in the UK: stations that recorded their maximum gusts within about half an hour of the passage of line B are labelled according to the hour when the peak gust occurred (a dot after the number indicates 30 minutes past the hour), and stations that recorded their maximum gusts after the passage of line C are simply labelled C. One station, labelled A, recorded its maximum gust at 0100 UTC during the passage of line A.*

a 48 m s^{-1} gust at 0400 UTC. The corresponding anemograph trace is shown in Figure 8a.

Figures 7a and b, respectively, show the E2- and E1-enhanced versions of the imagery for 0430 UTC, at which time many more chevron-shaped cloud features were evident, some obvious and others not so obvious. One particularly well-defined chevron can be seen with its leading edge crossing Kent. Figure 8b gives the anemograph trace for Ashford in mid-Kent and this shows that a maximum gust of 46 m s^{-1} (92 knots) broke the anemometer at 0435 UTC. Earlier less well-defined chevrons had crossed Kent at 0300 and 0330 UTC, producing maximum gusts of 39 and 37 m s^{-1}, respectively.

Some of the most damaging winds from this storm occurred in south-east England over the period 0300 to 0430 UTC in association with the chevron-shaped cloud features. Not all of the chevrons occurred in the area of strongest winds, however; for example, the chevron seen approaching Guernsey at 0430 UTC crossed Guernsey when the winds were generally subsiding and was associated with a peak gust of only 25 m s^{-1}. One might expect to be able to get a rough estimate of the severity of the gusts from the speed of travel of the chevrons. Unfortunately, the 30-minute interval between successive images was too large to be able confidently to track individual chevrons, which in many cases evolved beyond recognition over this interval. The major chevron that crossed Kent at 0430 UTC did appear to be more persistent than most but there was still ambiguity as to which of two features to match it with, thereby giving two alternative speeds of 35 and 55 m s^{-1} ($\pm$ 20%). The former speed seems implausibly slow bearing in mind that the mean

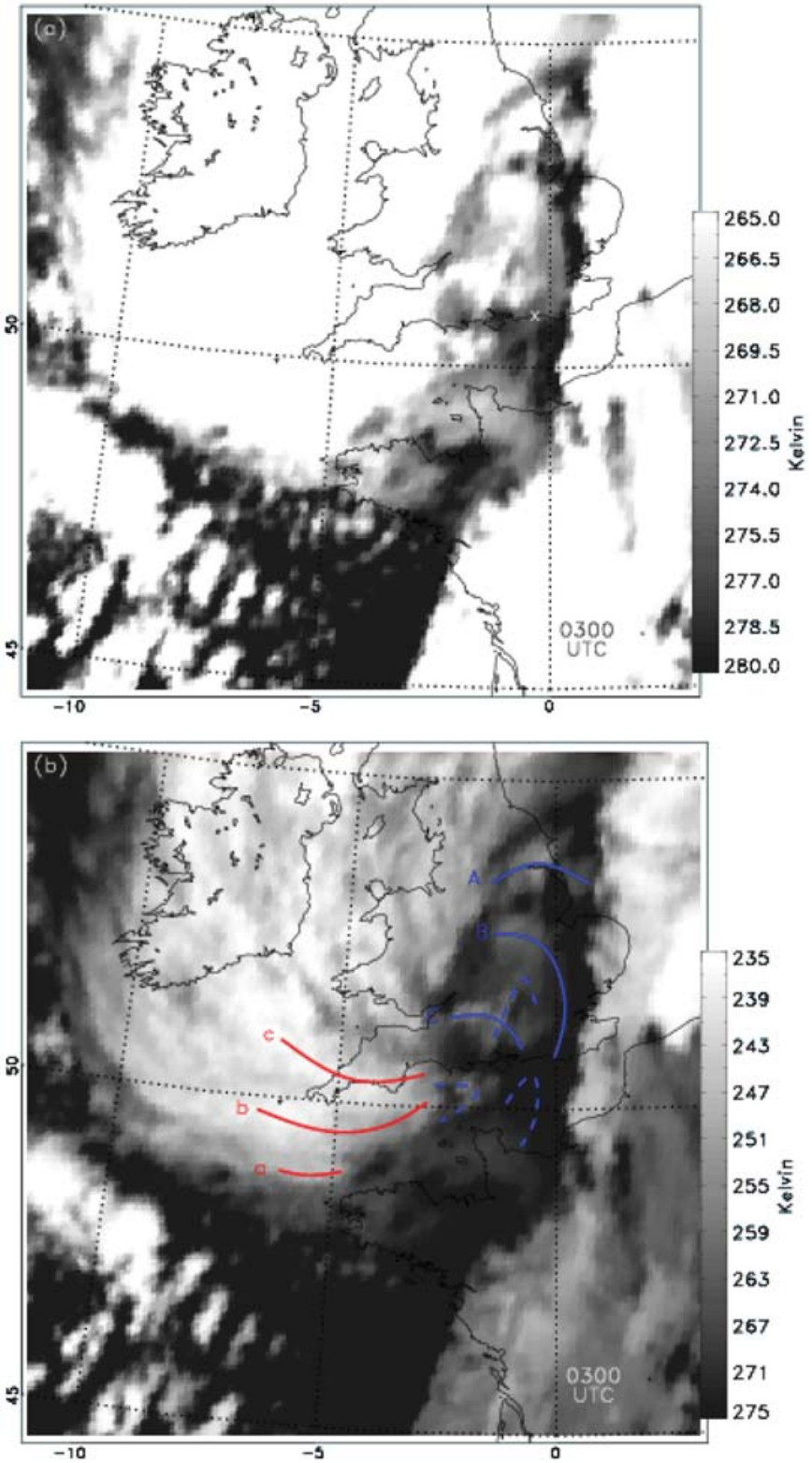

Figure 6. *Meteosat infra-red image for 0300 UTC, 16 October 1987 using (a) the E2 enhancement scheme and (b) the E1 enhancement scheme to bring out the structure of (a) the boundary-layer clouds and (b) the middle-and upper clouds. The red and blue lines in (b) represent, respectively, the axes of cloud-head bands, a′, b and c, and boundary-layer convergence lines inferred from low-level cloud features in (a). In addition to convergence lines A, B and C, additional boundary-layer cloud features are identified by dashed lines: these are the chevron-shaped clouds discussed in section 2.3. Note that cloud-head band a, strictly a′, is a newly developing band occurring close to the remnants of band a.*

speed at anemometer level was as high as 40 m s^{-1} at Ashford. On the other hand, 55 m s^{-1} seems rather high, and so perhaps even this chevron was evolving appreciably over the 30-minute interval. The tracings in Figure 7b suggest that adjacent chevrons overlapped one another and this could in itself account for some

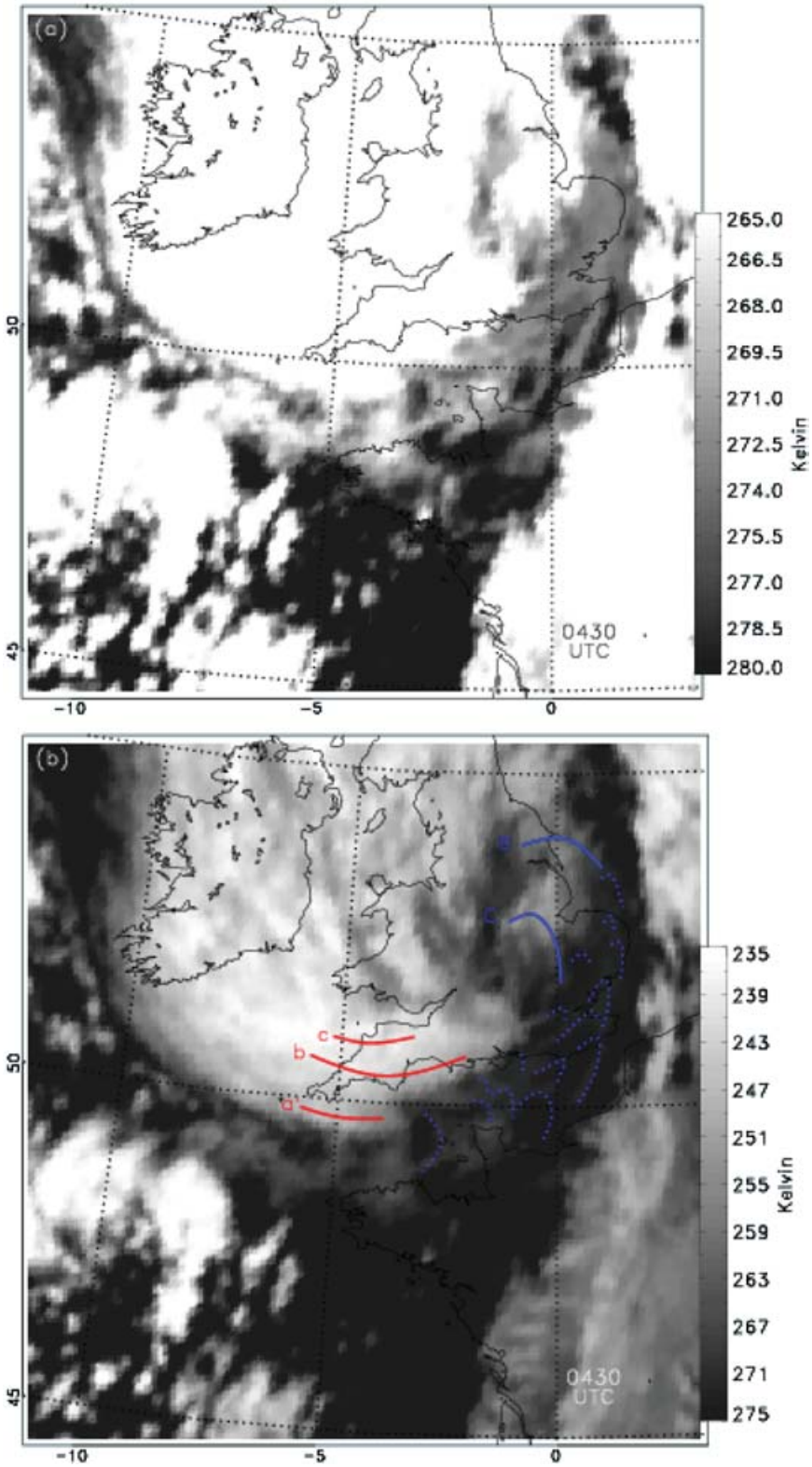

Figure 7. *As Figure 6 but for 0430 UTC. Many chevron-shaped boundary-layer clouds are evident crossing the English Channel and south-east England.*

of the evolution in the structure of the individual chevrons.

One structural feature that differentiated the Kent chevron, with its very strong surface gusts, from the Guernsey chevron, with its more modest surface gusts, is the pointedness of the chevron. Whereas the Guernsey chevron was a gentle curve, the Kent and neighbouring chevrons were shaped like arrowheads, giving the appearance of a ship's bow-wave. Like the larger arc-shaped cloud lines discussed in section 2.2, the chevrons occurred downwind of the cloud-head bands

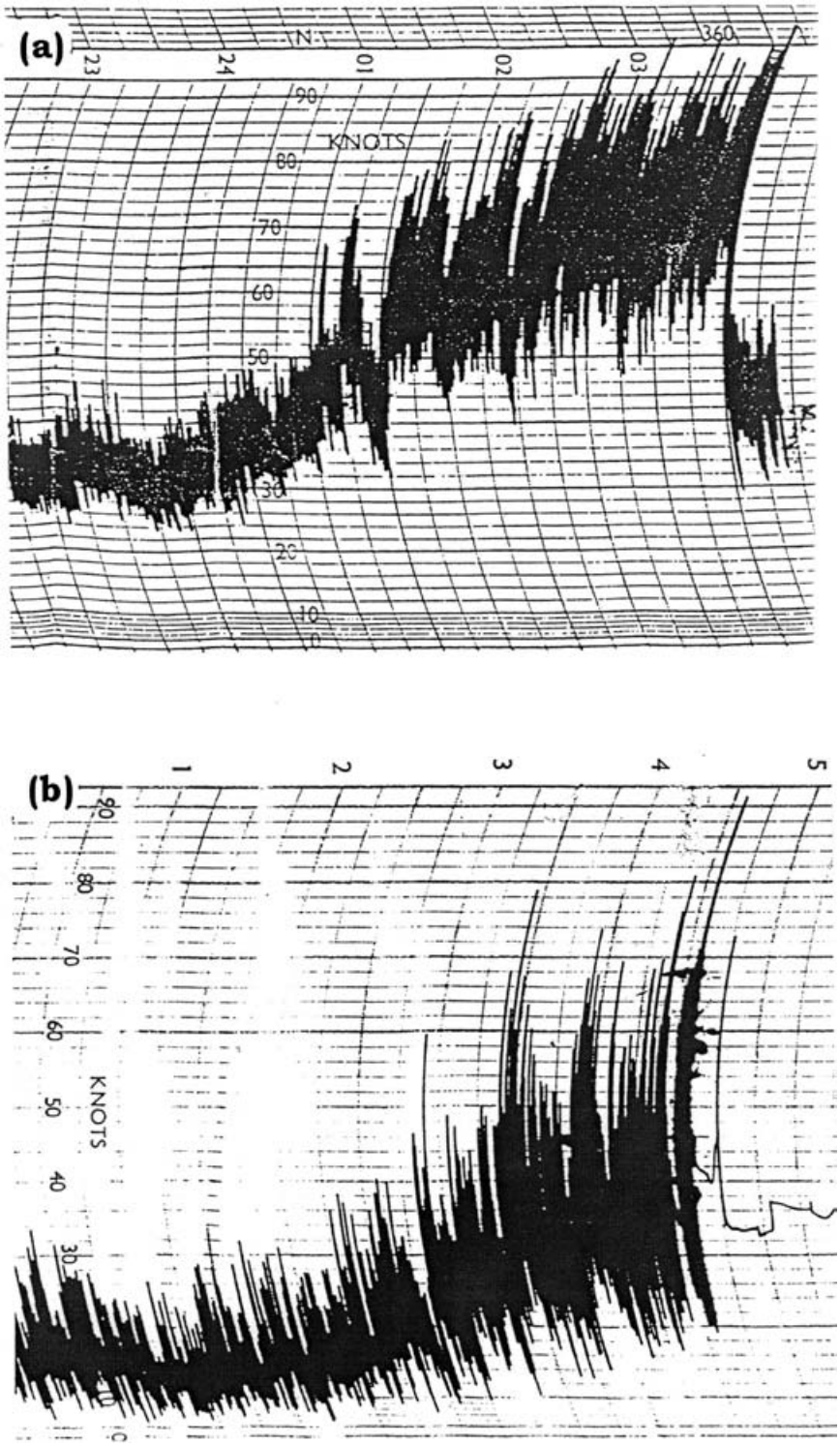

Figure 8. *Wind-speed traces from anemometers at (a) Shoreham Airport (50°50′N, 0°17′W) and (b) Headcorn Aerodrome, Ashford (Kent), before they were broken by severe gusts at 0400 UTC and 0434 UTC, respectively. There is a zero shift such that the speeds in (a) are 4 knots too high.*

and may have been related to the strongly descending sting-jet flows associated with them. It is, however, far from clear which cloud-head band they were associated with. Whereas the arc-shaped lines appeared to have time and space scales broadly matched to those of the major cloud-head bands (a, b, c), the shorter time and space scales of the chevrons suggest they may have been related to the rapidly evolving substructure within the cloud-head bands: Figures 3a and 3b illustrate well the fine-scale banded structure superimposed on the broad features labelled a, b and c. One is therefore led to speculate that the bow-wave-shaped chevron-clouds were the result of locally intensified regions of slantwise descent, which were embedded within the

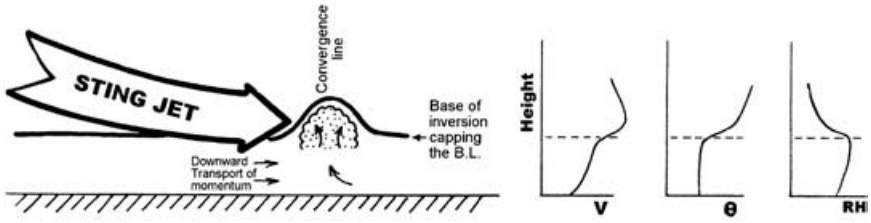

Figure 9. *Conceptual model of a dry, high-momentum sting-jet outflow interacting with a colder and relatively moist boundary layer to produce strong wind gusts at the surface just behind a convergence line detectable as a line of boundary-layer cloud.*

high-momentum sting jets, impacting at the top of the boundary layer. However, many of the chevrons were detected rather a long way ahead of the cloud-head band a′ and so one cannot altogether rule out the possibility that some of the chevrons in Figure 7 were the result of the impacts of intensified regions of slantwise descent that developed independently of the cloud-head bands.

3. A conceptual model for the generation of damaging winds by sting jets

This paper is one of a set of papers in which the mesoscale structure of the Great October 1987 storm is re-examined. The other papers have identified the existence and nature of the sting jets (Browning 2004; Clark & Browning 2004). Sting jets are composed of air that accelerates while descending within the cloud head and then exits at the tip of the cloud head where the cloud evaporates. The present study concentrates on the shallow cloud features that form within the dry slot where the sting-jet flows descend to the level of the boundary layer. By enhancing the infra-red imagery from Meteosat to bring out the structure of shallow low-level cloud, it has been possible to identify three kinds of cloud feature within the dry slot:

(1) a line of shallow (<5 km) cumulonimbus clouds,
(2) arcs of even shallower stratiform cloud, over 100 km long and confined within the boundary layer, and
(3) stratiform cloud features similar to (2) but chevron-shaped and only tens of kilometres across.

All of these clouds produced some rain, especially the cumulonimbus, and so the term 'dry slot' is relative. The cumulonimbus line has been analysed by Browning (2004) who suggested that it was triggered by a sting-jet outflow where it advances over residual high-θ_w air in the leading part of the dry slot. Some damaging wind gusts accompany the line of cumulonimbus, but by far the most damaging winds are associated with the non-convective boundary-layer cloud features identified as (2) and (3), especially (3). Understanding the behaviour of these non-convective boundary-layer cloud features constitutes the main thrust of the present paper.

The non-convective boundary-layer cloud systems are found downwind of the tip of the cloud head where multiple cloud-head bands terminate. The following set of hypotheses is proposed to link these cloud systems:

Hypothesis 1:

> Multiple cloud bands in the cloud head are associated with multiple slantwise circulations, the descending limbs of which constitute descending high-momentum flows referred to as sting jets (strictly speaking, multiple wind maxima within an overall sting jet).

Hypothesis 2:

> The arc and chevron cloud features in the dry slot are the result of boundary-layer convergence lines.

Hypothesis 3:

> There is a causal relationship between the multiple sting jets in Hypothesis 1 and the boundary-layer convergence lines in Hypothesis 2.

The physical reasoning underlying hypotheses 2 and 3 is embodied within Figure 9. Thermodynamic profiles for the region of the arc and chevron clouds, inferred from the modelling study of Clark & Browning (2004), are represented schematically on the right-hand side of Figure 9. They show an inversion separating a dry, high-θ, high-momentum airflow within the sting jet from relatively moist, low-θ air in the underlying boundary layer. In the leading part of the dry slot, where the cumulonimbus line forms, the inversion is obviously much weaker but in the region of the arc and chevron clouds, where the most damaging winds occur, the inversion is believed to be a significant feature. The capping inversion is not only a feature of the modelling study of Clark & Browning (2004) but it is also implied by the smooth-edged appearance of the observed boundary-layer cloud, especially that associated with the chevrons.

In view of the presence of an inversion, the question then arises as to how the sting jet interacts with the boundary layer to form the arc and chevron clouds.

The left-hand side of Figure 9 suggests that it does so by the downward transport of momentum through the boundary layer; this might be due to gravity-wave action and/or physical mixing as a result of shearing instability. The boundary-layer convergence that occurs at the leading edge of this region then leads to the arc and chevron clouds behind which there is a tendency for the cloud to dissipate owing to the downward mixing of dry air. This mixing is less marked where the sting jets overrun the warm seclusion, which is why the warm seclusion is able to persist. The mixing is stronger (and the clouds shallower) just to the south-east of the warm seclusion where the flow is colder and drier even at the surface, which is where the most damaging wind gusts are observed.

The tops of the chevron clouds are surprisingly high considering that they are confined to the boundary layer. In the case of the well-defined chevron that was crossing Kent when the Ashford anemometer was broken by a 46 m s^{-1} gust, the maximum brightness temperature was 272 K, which, assuming a θ_w of at least 283 K for the boundary-layer air, implies a cloud top of at least 2 km. This is to be compared with a boundary-layer depth of 1 to 1.5 km given by the numerical prediction model (Clark & Browning 2004) and suggests a substantial elevation of the boundary-layer top locally along the convergence line.

The interpretation of the boundary-layer cloud features in this study would have been easier and more convincing if it had been possible to resolve their structure better and, in particular, if it had been possible to track individual features such as the chevron clouds unambiguously between successive frames. The chevrons in the region where surface gusts exceeded 45 m s^{-1} had the appearance of ships' bow-waves: it is suspected that they represent the footprint of local maxima of momentum within the overrunning sting jets. An estimate of the speed of travel of the chevrons might be expected to give not only a measure of the magnitude of local wind maxima aloft but also an indication of the likely maximum gust velocities at the surface. Obtaining such estimates will be facilitated by the higher spatial resolution and 15-minute image intervals available from the

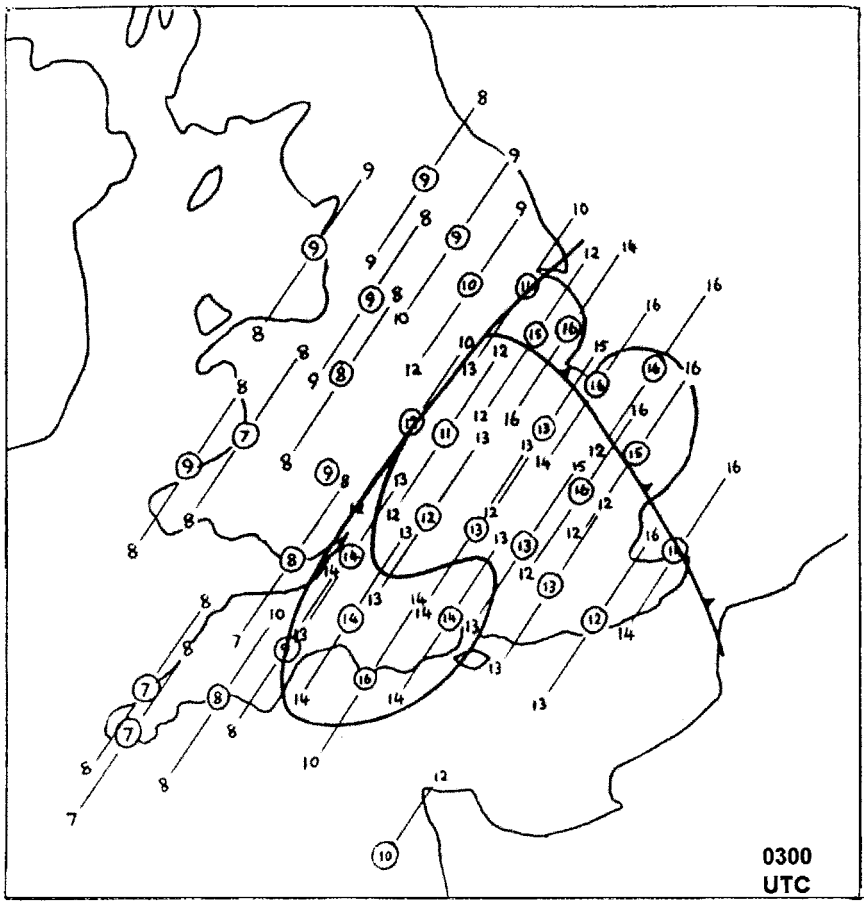

Figure A1. *Surface frontal analysis for 0300 UTC, 16 October 1987. Circles show locations of reporting stations. Hourly values of wet-bulb potential temperature for a given station, derived from hourly measurements as explained in the text, are connected by lines orientated along the direction of travel of the system. The front marked by cold-frontal symbols is the leading edge of cold downdraughts associated with the line of cumulonimbus, A; the other frontal lines represent the warm front and the bent-back front surrounding the warm seclusion which has just been cut off by cold air circulating around the south-eastern flank of the cyclone centred over Dorset.*

Meteosat Second Generation satellite. However, even 15-minute intervals may not be adequate for this purpose and so consideration should be given to arranging for rapid-scan (∼ 3-minute) sequences on appropriate occasions.

Acknowledgements

This research, carried out in the Joint Centre for Mesoscale Meteorology, is supported by the Met Office and the Department of Meteorology, University of Reading, and by the Universities Weather Research Network (UWERN), one of the Natural Environment Research Council Centres for Atmospheric Science. We are grateful to Chang-Gui Wang for her assistance in preparing the figures.

Appendix

Surface analyses

The surface frontal analyses shown in Figure 3 are based on a sequence of hourly analyses (not shown). An example of the raw data from which these analyses have been derived is given in Figure A1, which shows a plot of wet-bulb potential temperature values from 34 surface reporting stations. For each of these stations, time sequences of hourly readings for times T + 1, T and T − 1, where T = 0300 UTC, have been plotted as equivalent measurements in space, assuming to a first approximation that the overall pattern was frozen and travelling at 24 m s^{-1} from 215 deg.

References

Böttger, H., Eckardt, M. & Katergiannakis, U. (1975) Forecasting extratropical storms with hurricane intensity using satellite information. *J. Appl. Meteorol.* **14**: 1259–1265.

Browning, K. A. (2004). The sting at the end of the tail: damaging winds associated with extratropical cyclones. *Q. J. R. Meteorol. Soc.* **130**: 375–399.

Browning, K. A. & Roberts, N. M. (1994) Structure of a frontal cyclone. *Q. J. R. Meteorol. Soc.* **120**: 1535–1557.

Clark, P. A. & Browning, K. A. (2004) The sting at the end of the tail: model diagnostics of fine scale 3D structure of the cloud head. *Q. J. R. Meteorol. Soc.* submitted.

Grønås, S (1995) The seclusion intensification of the New Year's day storm 1992. *Tellus* **47A**: 733–746.

Shapiro, M. & Keyser, D. (1990) Fronts, jet streams and the tropopause. In *Extratropical Cyclones: The Eric Palmén Memorial Volume*, Am. Meteorol. Soc., Boston MA, pp. 167–191.